Monthly Notices of the ROYAL ASTRONOMICAL SOCIETY
MNRAS **491,** 4742–4751 (2020) doi:10.1093/mnras/stz3266
Advance Access publication 2019 November 21

Stellar cosmic rays as an important source of ionization in protoplanetary discs: a disc mass-dependent process

D. Rodgers-Lee,[1,2]★ A. M. Taylor,[3] T. P. Downes[4] and T. P. Ray[5]

[1] *School of Physics, Trinity College Dublin, University of Dublin, College Green, Dublin 2, Co. Dublin, D02 PN40, Ireland*
[2] *Centre for Astrophysics Research, School of Physics, Astronomy and Mathematics, University of Hertfordshire, College Lane, Hatfield AL10 9AB, UK*
[3] *DESY, D-15738 Zeuthen, Germany*
[4] *Centre for Astrophysics & Relativity, School of Mathematical Sciences, Dublin City University, Glasnevin, D09 W6Y4, Ireland*
[5] *School of Cosmic Physics, Dublin Institute for Advanced Studies, 31 Fitzwilliam Place, Dublin 2, D02 XF86, Ireland*

Accepted 2019 November 19. Received 2019 October 24; in original form 2019 August 8

ABSTRACT

We assess the ionizing effect of low-energy protostellar cosmic rays in protoplanetary discs around a young solar mass star for a wide range of disc parameters. We assume a source of low-energy cosmic rays located close to the young star that travels diffusively through the protoplanetary disc. We use observationally inferred values from nearby star-forming regions for the total disc mass and the radial density profile. We investigate the influence of varying the disc mass within the observed scatter for a solar mass star. We find that for a large range of disc masses and density profiles that protoplanetary discs are 'optically thin' to low-energy ($\sim$3 GeV) cosmic rays. At $R \sim 10$ au, for all of the discs that we consider ($M_{\rm disc} = 6.0 \times 10^{-4}$–$2.4 \times 10^{-2} {\rm M}_{\odot}$), the ionization rate due to low-energy stellar cosmic rays is larger than that expected from unmodulated galactic cosmic rays. This is in contrast to our previous results that assumed a much denser disc that may be appropriate for a more embedded source. At $R \sim 70$ au, the ionization rate due to stellar cosmic rays dominates in $\sim$50 per cent of the discs. These are the less massive discs with less steep density profiles. At this radius, there is at least an order of magnitude difference in the ionization rate between the least and most massive disc that we consider. Our results indicate, for a wide range of disc masses, that low-energy stellar cosmic rays provide an important source of ionization at the disc mid-plane at large radii ($\sim$70 au).

Key words: diffusion – turbulence – methods: numerical – protoplanetary discs – stars: low-mass – (ISM:) cosmic rays.

1 INTRODUCTION

Young low-mass stars are surrounded by discs of dust and gas, so-called protoplanetary discs. These discs evolve on a time-scale of a few Myrs and are known to accrete on to the central star. It seems likely that this accretion is facilitated via magnetic fields, either the magnetorotational instability (MRI; Balbus & Hawley 1991) and/or magnetocentrifugally launched winds (Blandford & Payne 1982). Both of these magnetically driven physical processes require a certain level of ionization for the neutral material to effectively couple to the magnetic field via ionized charge carriers.

Indeed, the nature of this coupling between the field and the bulk fluid is critically dependent on the ionization fraction, with Ohmic resistivity, the Hall effect and ambipolar diffusion all thought to be important in different parts of the disc (Wardle 2007). Much work has been published on the impact of these effects on global disc dynamics: O'Keeffe & Downes (2014) using multifluid magnetohydrodynamic (MHD) simulations and Lesur, Kunz & Fromang (2014) using single-fluid MHD simulations were the first to explore the dynamics of protoplanetary discs in the presence of all three of these effects, while others (e.g. Bai 2014; Gressel et al. 2015; Rodgers-Lee, Ray & Downes 2016; Béthune, Lesur & Ferreira 2017) followed up with explorations of disc dynamics and wind launching with a variety of distributions for the non-ideal MHD effects in the disc. Since the size of the three relevant non-ideal MHD effects is so dependent on the ionization fraction, all of these works suffer from the large existing uncertainty in the ionization rate. Thus, determining the sources of ionization in protoplanetary discs is of great importance.

While stellar X-rays (Ercolano & Glassgold 2013) and radioactivity (Umebayashi & Nakano 2009) offer a certain amount of ionization they fail to sufficiently ionize deep into the disc, in the region therefore commonly known as the dead-zone (Gammie 1996). Due to the possibility that Galactic cosmic rays are suppressed by the young star's heliosphere (as noted by Gammie 1996; Glassgold,

★ E-mail: drodgers@tcd.ie

Najita & Igea 1997; Cleeves, Adams & Bergin 2013) some interest has been generated concerning the ionizing effect of low-energy cosmic rays (∼GeV energies) produced by the young star itself (Turner & Drake 2009; Rab et al. 2017; Rodgers-Lee et al. 2017; Fraschetti et al. 2018).

Stellar cosmic rays may be able to ionize the protoplanetary disc sufficiently to decrease the extent of the dead-zone. Therefore, the MRI may operate in larger regions of the disc than previously thought. This additional source of ionization might also help to launch magnetocentrifugally winds at lower heights above the disc mid-plane.

The ionization rate in protoplanetary discs is a difficult quantity to observationally constrain and yet remains the clearest indication of the presence of low-energy cosmic rays, especially if other sources of ionization in the system can simultaneously be accounted for. Cleeves et al. (2015) present a constraint on the total ionization rate for TW Hya ($\zeta \lesssim 10^{-19}\mathrm{s}^{-1}$) using chemical modelling of HCO^+ and N_2H^+ observations. On the other hand, Schwarz et al. (2018) find that it is difficult to model current CO observations that find low CO abundances without cosmic rays (Galactic or otherwise) or UV photons. It is possible that low-energy stellar cosmic rays could play a role in explaining these CO observations. Further away from the protoplanetary disc, Ainsworth et al. (2014) have found indications of non-thermal processes occurring in the jet bow shocks from young low-mass stars.

On the theoretical side, there has been much interest in the acceleration of stellar cosmic rays and their subsequent transport. Padovani et al. (2015) and Padovani et al. (2016) investigated possible acceleration sites in the vicinity of young stellar objects. Padovani et al. (2018) investigated the energy-loss processes of galactic cosmic rays in very dense media that lead to higher ionization rates as a function of grammage than expected from previous calculations (such as Umebayashi & Nakano 1981) which is also relevant for stellar cosmic rays. On a more global scale, Gaches & Offner (2018) estimated the ionization rate in star-forming molecular clouds due to energetic particles accelerated in the accretion columns of young stellar objects.

Regarding the transport of stellar cosmic rays, Rodgers-Lee et al. (2017), Rab et al. (2017), and Fraschetti et al. (2018) all found that low-energy stellar cosmic rays injected near the star were unable to travel far into the protoplanetary disc. In the first case, the cosmic rays lost their energy due to the high density in the inner regions of the disc near the mid-plane despite the assumption of diffusive transport. In Rab et al. (2017), rectilinear transport was assumed for mainly MeV cosmic rays. Thus, the combination of very low-energy cosmic rays (which have high-energy loss rates) with the geometric dilution factor of $1/r^2$ caused the cosmic rays to be attenuated significantly. Last, Fraschetti et al. (2018) using test particle simulations found that stellar cosmic rays were magnetically confined due to the stellar magnetosphere.

It is important to note that these simulations all use a different value for the mass of the central star. Rodgers-Lee et al. (2017), Rab et al. (2017), and Fraschetti et al. (2018) use $M_* = 1$, 0.7 and $1.35(\pm 0.15)\,\mathrm{M}_\odot$ for the young star, respectively. For Rodgers-Lee et al. (2017) and Rab et al. (2017), who implement a density profile for the disc, the scale height of the disc is dependent on the mass of the central star that will affect the absorption of the stellar cosmic rays.

As noted above each of these models assumed a different mass for the central star. Other differences also exist concerning the mass and density structure of the disc itself. The density profile used in Rodgers-Lee et al. (2017) is a radial power-law profile (their equation 7) with an exponential drop-off in the vertical direction. Rab et al. (2017) use a similar expression for the density profile but with a tapering-off radius at 100 au and a disc mass of $0.01\,\mathrm{M}_\odot$. On the other hand, Fraschetti et al. (2018) assume a more simplified disc model that lies in the *xy*-plane and has no vertical or radial density structure.

The aim of this paper is to build on our previous work assuming diffusive transport and to investigate different disc masses and density profiles based on physical parameters from current observations. We then examine the range of parameters that can increase the ionization rate deep in the disc. The model and parameters used are described in Section 2. In Section 3, we present our results and discuss them in the context of our previous findings, as well as in comparison to the literature, in Section 4. Finally, we outline our conclusions in Section 5.

2 FORMULATION

We use the same model as described in Rodgers-Lee et al. (2017). Namely, we assume diffusive transport for the low-energy cosmic rays and solve the associated 2D transport equation

$$\frac{\partial n_{\mathrm{CR}}}{\partial t} = \nabla \cdot (D \nabla n_{\mathrm{CR}}) - \frac{n_{\mathrm{CR}}}{\tau} + Q, \tag{1}$$

where n_{CR} is the number density of cosmic rays, $D(R, z)$ is the spatial diffusion coefficient, $1/\tau(R, z)$ is the cosmic ray energy-loss rate [given by equation 6 in Rodgers-Lee et al. (2017) and is related to the mass density of the protoplanetary disc], and Q is the injection rate of low-energy cosmic rays. Q is linked to the luminosity of low-energy cosmic rays that we assume which is given in Section 2.3.1. The assumed diffusion coefficient is also given in Section 2.3.1. It is important to note that we do not consider an advective term here since we investigated this previously and found it to have little effect. Equation (1) is solved using cylindrical coordinates assuming axial symmetry. Further details regarding the code are given in Rodgers-Lee et al. (2017).

2.1 The diffusive approximation

The assumption of diffusive transport for cosmic rays is relevant if the cosmic rays are travelling through a magnetized medium and when some level of turbulence is present in the magnetic field. This turbulence in the magnetic field prevents the cosmic rays from travelling in straight lines (which would happen, for instance, if no magnetic field was present or if it is sufficiently weak in comparison to the energy of the cosmic rays, such as in Rab et al. 2017). It also means that the cosmic rays are not entirely tied to magnetic fields (such as found in Fraschetti et al. 2018). Instead, they scatter off perturbations in the magnetic field structure leading to the cosmic rays diffusing through the system.

In a spherically symmetric system, and if the cosmic ray energy losses are negligible, then the analytic result for diffusive transport gives a $1/r$ profile. In comparison ballistic propagation, without energy losses, gives a $1/r^2$ profile. Therefore, assuming the same density of cosmic rays at 1 au for instance, means that if the cosmic rays are diffusing then at 100 au the density of cosmic rays will be 100 times larger than if they move ballistically. If energy losses become dominant then the radial profile of cosmic rays will deviate from the $1/r$ profile. Fig. 5.6 of Longair (2011) shows the rate at which cosmic rays of different energies loss energy, as they travel ballistically through different media. In the context of diffusive transport, it is important to remember that the cosmic rays are random walking through the disc. As a result the vertical or radial column density of protoplanetary discs does not relate to the path that the cosmic rays have taken through the disc, and therefore, the amount of material that they have passed through to travel out to any given radius. Thus, the column density of the disc is no longer a meaningful quantity to consider. Therefore, we consider the ionization rates resulting from stellar cosmic rays as a function of radius instead.

2.1.1 Observations of magnetic fields in protoplanetary discs

Observationally measuring either the magnetic field structure or its strength in protoplanetary discs has proved immensely challenging. Donati et al. (2005) reported the direct detection of the magnetic field in the core of the protostellar accretion disc of FU Orionis with the high-resolution spectropolarimeter ESPaDOnS. The magnetic field strength reaches strengths of ∼1 kG close to the centre of the disc. This is obviously a very strong magnetic field and is partially why FU Orionis was chosen as a target, but FU Orionis is not a typical classical T-Tauri star (CTTS). None the less, this detection supports the idea that magnetic fields are present in protoplanetary discs. If the low-energy cosmic rays are ejected outside of the young star's magnetosphere, thus ensuring their escape, it is reasonable to assume that some level of turbulence exists in the magnetic field threading the protoplanetary disc and thus it is valid to assume diffusive transport.

2.2 Initial conditions

We expand our previous model so that we can study spatially larger discs, comparable in size to the best studied ALMA samples (Ansdell et al. 2016; Tazzari et al. 2017), with a large range of disc masses and surface density profiles. We implemented a logarithmic grid to be able to extend the computational grid in both the r- and z-direction to ∼100 au. The number of cells in both the radial and vertical direction is $N_{\rm r} = N_{\rm z} = 60$ giving sufficient spatial resolution for numerically converged results (a convergence test is given in the Appendix). At the same time, this relatively small number of cells allows us to run many simulations varying the disc mass and the radial power-law index that are described in the following sections.

To avoid imposing a small time-step constraint when using the logarithmic grid we set the inner edge of the computational domain to be $R_{\rm min} = z_{\rm min} = 0.1$ au. Previously the injection site of low-energy cosmic rays was taken to be the magnetospheric truncation radius, $R \sim 0.07$ au at a height of $z = 0.03$ au above the disc mid-plane. Now since $R_{\rm min} = z_{\rm min} = 0.1$ au, we inject the cosmic rays at $(r, z) = (0.14$ au, 0.14 au). We checked the effect of changing the injection position of the cosmic rays and found it had little effect. It is also important to note that by using $R_{\rm min} = z_{\rm min} = 0.1$ au we are limited to examining the effect of the cosmic rays at heights $\gtrsim 0.1$ au above the disc mid-plane.

The outer radial and vertical boundary conditions are absorptive that allow the cosmic rays to diffuse out of the system. The inner radial and vertical boundary conditions are reflective, since we assume symmetry about the disc mid-plane and axial symmetry about the axis of rotation of the disc. The following sections describe the range of values for the physical parameters that we consider for the low-energy stellar cosmic rays and for the disc.

2.3 Physical parameters

In this section, we describe the properties that we use for the low-energy cosmic rays. We also outline how we vary the disc mass and the radial density profile, motivated by current observations, in order to investigate the ionizing influence of stellar cosmic rays in protoplanetary discs.

2.3.1 Energy and diffusion coefficient of the cosmic rays

We assume 3 GeV cosmic rays (protons) and a diffusion coefficient of $D/c = 30r_{\rm L}$, where $r_{\rm L}$ is the Larmor radius of the particle. We have assumed an mG magnetic field in the calculation of the Larmor radius. This value for the diffusion coefficient is the same as for the fiducial case presented in Rodgers-Lee et al. (2017). The transport properties of low-energy cosmic rays in MRI turbulence are unknown and so we can only constrain the diffusion coefficient to be above the Bohm limit, i.e. $D/c > r_{\rm L}$, where the diffusion approximation is valid. While we only investigate here the influence of 3 GeV low-energy cosmic rays we still choose a diffusion coefficient for a 3 GeV proton such that the diffusion coefficient for MeV protons remains above the Bohm limit, since the diffusion coefficient scales with momentum (see equation 5 of Rodgers-Lee et al. 2017). For simplicity, we assume mono-energetic cosmic rays of 3 GeV.

In Section 4, we briefly discuss the effect of varying the diffusion coefficient on the results presented in Section 3 that assume $D/c = 30r_{\rm L}$. In Section 4, we also discuss the effect of including an energy spectrum of cosmic rays based on our previous findings in Rodgers-Lee et al. (2017). The luminosity of the low-energy cosmic rays is taken to be $L_{\rm CR} = 1 \times 10^{28}\,{\rm erg\,s^{-1}}$, as in Rodgers-Lee et al. (2017).

2.3.2 Disc mass

For our simulations of cosmic-ray propagation, the gas mass density of the disc (rather than the dust mass density) is the important quantity since the bulk of the disc mass resides in the gas. This is true if we assume the canonical interstellar medium (ISM) value of 100 for the dust-to-gas mass ratio. However, while there are a large number of discs with measured dust masses, measuring the gas disc mass has proved more difficult than anticipated (for instance, with ALMA CO observations; Miotello et al. 2017). Therefore, we infer a total disc mass by examining the dust disc masses for which there are larger observational data sets available. We assume that the measured dust mass is a fixed fraction (1/100) of the total mass of the disc.

Observations of protoplanetary discs have shown that the dust disc mass for a given stellar mass displays a large dispersion (fig. 7 of Pascucci et al. 2016 for instance). To calculate a dust disc mass these observations assume that the dust emission is optically thin, isothermal, and adopt a particular value for the dust opacity. None the less, variation of these parameters is not sufficient to reproduce the scatter observed for the disc mass versus stellar mass relationship. This scatter is observed across different star-forming regions, as well as within individual regions.

We use the relationship given in Pascucci et al. (2016) for the dust disc mass as a function of stellar mass that we rearrange to express the total disc mass, $M_{\rm disc}$, as

$$M_{\rm disc} = 3 \times 10^{-4} \left[10^{1.1\pm0.8} \left(\frac{M_*}{\rm M_\odot} \right)^{1.9} \right] {\rm M_\odot}. \qquad (2)$$

This relation is derived from observations of the ∼2 Myr old Chamaeleon star-forming region. For much younger or older star-forming regions the relationship would be different. In equation (2), we have adopted the maximum dispersion (0.8) found for the observations which is thought to represent real physical scatter. Thus, we can examine the effect of varying $M_{\rm disc}$ for a given stellar mass. Taking $M_* = 1\mathrm{M}_\odot$, we have $M_{\mathrm{disc,min}} = 6.0 \times 10^{-4}\mathrm{M}_\odot$ and $M_{\mathrm{disc,max}} = 2.4 \times 10^{-2}\mathrm{M}_\odot$ with a mean value of $3.8 \times 10^{-3}\mathrm{M}_\odot$.

2.3.3 *Normalizing density, ρ_0*

The disc mass is calculated from the gas density profile of the disc as

$$M_{\mathrm{disc}} = 2 \int_{z_{\mathrm{min}}}^{z_{\mathrm{max}}} \int_{R_{\mathrm{min}}}^{R_{\mathrm{out}}} 2\pi R\, \rho(R, z)\, \mathrm{d}R\, \mathrm{d}z. \quad (3)$$

The factor of 2 in this equation is due to our assumption of symmetry about the disc mid-plane. Observations of R_{out} for the gaseous disc give $R_{\mathrm{out}} \sim 70$–460 au (Ansdell et al. 2018, for 22 discs in the Lupus star-forming region). A fiducial value for the disc outer radius $R_{\mathrm{out}} = 100$ au is used for all of the simulations and we also set $z_{\mathrm{max}} = R_{\mathrm{out}}$. The inner boundaries, R_{min} and z_{min}, are set to 0.1 au as described in Section 2.2. It is important to note that ALMA surveys focusing on the gas discs, as mentioned in Ansdell et al. (2018), are biased towards the highest mass discs and thus it is possible that lower mass discs with smaller radii are common but undetected by ALMA.

The gas density profile in equation (3) (as in Rodgers-Lee et al. 2017) is given by

$$\rho(R, z) = \rho_0 \mathrm{e}^{-R_{\mathrm{in}}^2/R^2} \left(\frac{R}{R_0}\right)^{-p} \mathrm{e}^{-z^2/2H^2} + \rho_{\mathrm{ISM}}, \quad (4)$$

where ρ_0 is the normalizing density at $R_0 = 1$ au at the mid-plane of the disc. $R_{\mathrm{in}} = 0.07$ au is the inner edge of the disc which is taken to be the truncation radius for a typical CTTS (the value for R_{in} is described in more detail in Rodgers-Lee et al. 2017). It is important to note that R_{in} is not the same as R_{min}. As mentioned in Section 2.2, $R_{\mathrm{min}} = 0.1$ au slightly larger than R_{in} to avoid a small time-step. $\rho_{\mathrm{ISM}} = 3.89 \times 10^{-24}\,\mathrm{g\,cm^{-3}}$ is the density of the ISM and $H = c_\mathrm{s}/\Omega$ is the scale height of the disc where c_s is the sound speed and Ω is the Keplerian frequency. The temperature profile used for calculating the sound speed, c_s, is given by

$$T(R) = T_0 \left(\frac{R}{R_0}\right)^{-q}, \quad (5)$$

where $T_0 = T(R_0) = 280$K and $q = 0.5$ for a solar mass star.

Equations (3)–(4) show that M_{disc} can be varied most by varying the following two parameters: the radial power-law index, p, and the normalizing density, ρ_0 since we have chosen a fiducial value of $R_{\mathrm{out}} = 100$ au. The resulting values of ρ_0 chosen to give the minimum, mean and maximum disc masses (for the mean value of $p = 1.25$ which is discussed in Section 2.3.4) given in Section 2.3.2 are $\rho_0 = 1.0 \times 10^{-13}$, 6.8×10^{-13}, and $4.35 \times 10^{-12}\,\mathrm{g\,cm^{-3}}$, respectively. In the following section, we will discuss the range of values that we consider for the radial power-law index, p.

2.3.4 *Radial power-law index*

As mentioned above, the radial power-law index, p, in equation (4) is important in determining the density profile of protoplanetary discs. Observations can probe the dust surface density power-law index, γ (Tazzari et al. 2017, for instance) more easily than the gas surface density, where the dust surface density profile can be described by

$$\Sigma(R) = \Sigma_0 \left(\frac{R}{R_0}\right)^{-\gamma}. \quad (6)$$

Integrating over z in equation (4) [and assuming a power law distribution for the temperature profile for the disc which only depends on radius such as equation (5)] links the power-law indices in $\Sigma(R)$, $T(R)$, and $\rho(R, z)$ such that $\gamma = p - 3/2 + q/2$.

Tazzari et al. (2017) observationally constrain γ for 22 (dust) discs around low-mass stars ($\sim$0.1–2.0$\mathrm{M}_\odot$) in the Lupus star-forming region from their ALMA survey at 890 μm. Instead of using equation (6) exactly they in fact also include an exponential cut-off in the disc surface density characterized by R_c, as in their equation (1). However, if $R_\mathrm{c} > R_{\mathrm{out}}$ then these equations are very similar.

Tazzari et al. (2017) find a distribution of values for γ centred around $\gamma = 0$ with a standard deviation of 0.6. For our simulations, we look at the gas density and therefore, lacking better information, we assume that the gas and dust have the same density profiles. Thus, $-0.6 \le \gamma \le 0.6$, motivated by observations, gives $0.65 \le p \le 1.85$, assuming $q = 0.5$. For the MMSN model $\gamma = 1.5$ and $p = 2.75$, again assuming $q = 0.5$. Thus, we investigate $0.65 \le p \le 2.75$ to extend the range to include the values used in the MMSN model. In Rodgers-Lee et al. (2017), we investigated $0.5 \le p \le 1.5$ which are similar to the values inferred from observations.

2.4 The simulations

We study the effect of varying the disc mass and of varying p via a parameter space survey. We choose 12 logarithmically spaced disc masses in the range $M_{\mathrm{disc}} = 6 \times 10^{-4}$–$2.4 \times 10^{-2} M_\odot$. For each of these 12 disc masses, we perform simulations for 15 linearly spaced values of p in the range of 0.65–2.75 (described above). The results presented in the next section are based, therefore, on a suite of 180 separate simulations.

3 RESULTS

In this section, we present the results from our simulations. In Sections 3.1–3.4, we will first begin by discussing a number of specific simulations in detail. Namely, the results relating to the mean, minimum, and maximum disc mass simulations. We will also present results for the mean disc mass for varying density profiles. We will discuss the results obtained for the disc parameters most similar to those of the MMSN. Finally, we present a more general view of the results in Section 3.5.

The main diagnostic that we examine is the ionization rate, ζ_{CR}, resulting from low-energy stellar cosmic rays. The ionization rate is calculated using equation 15 of Rodgers-Lee et al. (2017) which is based on equation 21 of Umebayashi & Nakano (1981). It is important to note that, as discussed in Section 2.2, the smallest vertical height above the disc mid-plane that we can examine the ionization rate at is $\sim$0.14 au. In comparison, in Rodgers-Lee et al. (2017) we were able to investigate a smaller vertical height above the disc mid-plane of 0.03 au. At small radii ($\lesssim 0.5$ au), the vertical density profile changes rapidly since the scale height of the disc is small. Thus, the ionization rate at 0.14 au above the disc mid-plane may differ from the ionization rate at the disc mid-plane. In fig. 4 of Rodgers-Lee et al. (2017), the black and blue dots show the ionization rate as a function of radius at a height of 0.03 and 0.1 au above the disc mid-plane, respectively. For radii < 0.1 au, the ionization rate differs by approximately a factor of 2 for the different vertical heights above the disc mid-plane. At 1 au, there is approximately a factor of 3 difference between the ionization rates but this gradually decreases for larger radii. At large radii, the change in the density of the disc at the mid-plane and at 0.14 au

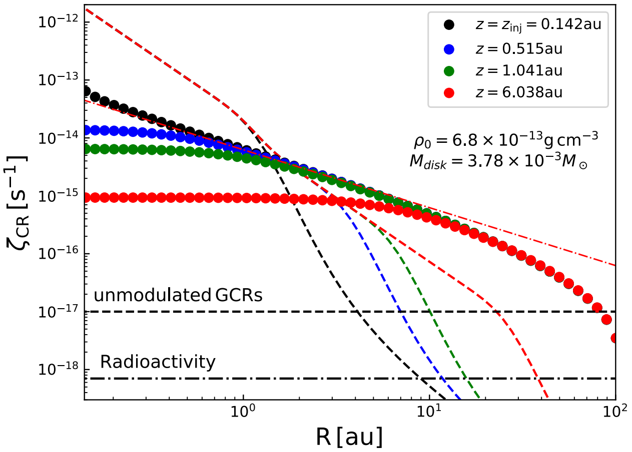

Figure 1. This plot shows the ionization rate due to 3 GeV low-energy cosmic rays as a function of radius for varying heights above the mid-plane of the disc. The disc mass for this simulation is the mean disc mass described in Section 2.3.2 and the radial density profile has $p = 1.25$ in equation (4). The assumed value of ρ_0 is indicated on the plot. The red dash–dotted line indicates the analytic result for spherically symmetric diffusion, without considering any energy losses. The ionization rate expected from unmodulated galactic cosmic rays and also from radioactivity are shown on the plot for comparison. The dashed lines represent the ionization rate from stellar X-rays for the same heights above the disc mid-plane as for the stellar cosmic rays.

above the disc mid-plane will be relatively small. Therefore, at large radii examining the ionization rate at 0.14 au above the disc mid-plane will be a good estimate of the ionization rate at the disc mid-plane.

3.1 Mean $M_{\rm disc}$ and mean value of p

We start by examining the ionization rate from low-energy cosmic rays obtained for the simulation with the most typical disc parameters (motivated by observations): the mean disc mass ($M_{\rm disc} = 3.78 \times 10^{-3}M_\odot$) and the mean value of $p = 1.25$. These values result in $\rho_0 = 6.8 \times 10^{-13}$g cm^{-3}. Fig. 1 shows the resulting ionization rate as a function of radius in the disc for different vertical heights above the disc mid-plane. For reference, the ionization rate expected from unmodulated galactic cosmic rays ($\zeta_{\rm GCR} \sim 10^{-17}$ s^{-1}, Umebayashi & Nakano 1981) and radioactivity (7×10^{-19} s^{-1}, Umebayashi & Nakano 2009) are given by the black dashed and dash–dotted lines, respectively. The dashed lines represent the ionization rate from stellar X-rays for different vertical height above the disc mid-plane, using the same parametrized fit from Bai & Goodman (2009), as used in Rodgers-Lee et al. (2017). The assumed X-ray luminosity is 10^{29}erg s^{-1}.

The first most noticeable result in Fig. 1 is that the $1/r$ profile expected from spherically symmetric spatial diffusion (in the absence of losses) is recovered out to ∼10 au at the disc mid-plane, as indicated by the black points. The red dash–dotted line indicates the analytic result for spherically symmetric diffusion, without considering any energy losses. The black points trace the ionization rate at a vertical height of 0.142 au above the disc mid-plane. This result is significantly different from our previous findings in Rodgers-Lee et al. (2017), where we found that the cosmic rays were strongly attenuated within ∼1 au and had a much steeper than $1/r$ profile. We discuss in detail the reasons for this difference in Section 4. Essentially, though this difference merely represents a difference in the underlying assumed density profile of the disc.

The second interesting result is that the ionization rate resulting from low-energy stellar cosmic rays is larger than the ionization rate expected from unmodulated galactic cosmic rays out to ∼80 au at a vertical height of 0.142 au above the disc mid-plane. The ionization rate from stellar cosmic rays also dominates over the contribution from stellar X-rays beyond ∼4 au. This indicates that for this 'typical' disc low stellar energy cosmic rays can result in high levels of ionization deep within the disc out to ∼80 au.

The blue, green and red points show the ionization rate at increasing heights above the disc mid-plane in Fig. 1. As expected, at small radii but high above the disc mid-plane the ionization rate is smaller than for lower heights. For $R \gtrsim 10$ au, the ionization rate is the same irrespective of the height above the disc mid-plane. The lower ionization rates displayed at large vertical heights (the red dots out to ∼10 au for instance) occur at large values of z/R. This merely reflects that the spherical radius is then significantly larger the cylindrical radius at these heights and radii. The ionization rate is in fact nearly spherically symmetric which implies that this particular disc is, for the most part, 'optically thin' to the cosmic rays.

Another interesting quantity to examine is the ionization fraction which can be used to determine the level of coupling between the neutral and charged species. This level of coupling is important to determine for non-ideal magneto-hydrodynamic simulations of protoplanetary discs. Based on the simplified chemical network from Fromang, Terquem & Balbus (2002), we can estimate the ionization fraction using equations (16)– (17) of Rodgers-Lee et al. (2017) by choosing an appropriate recombination rate coefficient.

We consider two extreme cases which represent when metals are present or absent in the gas. If the metal ions are locked in sedimented grains we calculate the ionization fraction at $z = 0.142$ au above the disc mid-plane to be 6.3×10^{-9}, 1.2×10^{-10}, 1.1×10^{-10} and 7.8×10^{-11} at $R = 1$, 10, 30, and 70 au, respectively. If metal ions instead dominate as charge carriers in the plasma then we find that the ionization fraction at $z = 0.142$ au above the disc mid-plane to be 1.8×10^{-6}, 3.9×10^{-8}, 3.5×10^{-8}, and 2.5×10^{-8} at $R = 1$, 10, 30, and 70 au, respectively.

The ratio of neutral-ion collision time in comparison to the orbital time gives an estimate of the level of coupling between the ions and the neutral gas that can be used as a criteria to determine whether the MRI will be active or not in the disc (equation 2 from Chiang & Murray-Clay 2007, for instance). This ratio depends on the ionization fraction in the disc. For the ionization fractions given above, we find that if metal ions are locked in sedimented grains the neutral-ion coupling is poor. On the other hand, we find, if metal ions dominate as charge carriers, that the ionization fractions recovered due to stellar cosmic rays may be important for the dynamics of protoplanetary discs since the neutral-ion collision time is sufficiently small in comparison to the orbital time.

3.2 Minimum and maximum values of $M_{\rm disc}$ with $p = 1.25$

Next, we examine the effect of varying the disc mass from the minimum ($M_{\rm disc} = 6 \times 10^{-4}M_\odot$) to the maximum ($M_{\rm disc} = 2.4 \times 10^{-2}M_\odot$) values that we motivated in Section 2. We keep $p = 1.25$ fixed here. The resulting ionization rate profiles for the minimum, mean, and maximum disc masses are shown in Fig. 2. For the minimum disc mass simulation the ionization due to low-energy cosmic rays now results in $\zeta_{\rm CR} > 10^{-17}$s^{-1} effectively throughout the whole disc (blue dots in Fig. 2). On the other hand, as expected, for the maximum disc mass case the stellar cosmic rays are more

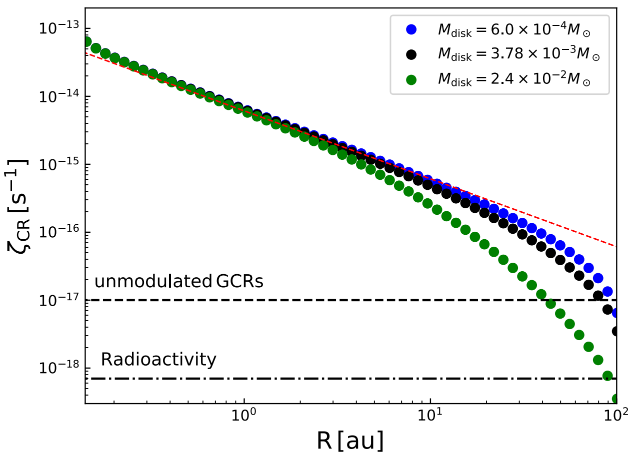

Figure 2. This plot shows the ionization rate as a function of radius at $z = 0.142$ au above the mid-plane of the disc for the minimum, mean and maximum disc masses examined here using the mean value of $p = 1.25$ for all three cases.

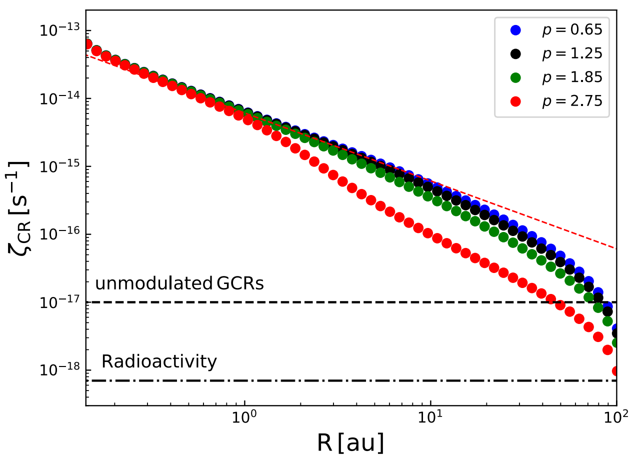

Figure 3. This plot shows the effect of varying the density profile on the resulting ionization rate for the mean disc mass ($M_{disc} = 3.78 \times 10^{-3}\,M_\odot$). The ionization rate is given as a function of radius at $z = 0.142$ au above the mid-plane of the disc.

attenuated, such that at ∼2 au the ionization rate profile is steeper than $1/r$ (green dots in Fig. 2). None the less, for the typical most massive disc that we consider the low-energy cosmic rays still outcompete the unmodulated galactic cosmic ray ionization rate out to a radius of ∼40 au for all heights above the disc. Beyond $R \gtrsim 20$ au at the disc mid-plane, the difference in the resulting ionization rate between the most massive disc and the least massive disc is approximately an order of magnitude.

3.3 Mean disc mass with varying density profiles

In this section, we focus on the effect of varying the density profile of the disc while keeping the disc mass fixed as the mean disc mass. We varied $p = 0.65$–2.75, where the range of $p = 0.65$–1.85 is motivated by observations and the additional values up to $p = 2.75$ reflects our interest in considering discs with parameters similar to those of the MMSN disc that has $p = 2.75$.

Fig. 3 shows the radial ionization rate profiles considering the mean disc mass with $p = 0.65$–2.75. For $p = 0.65$ and $p = 1.85$ (the

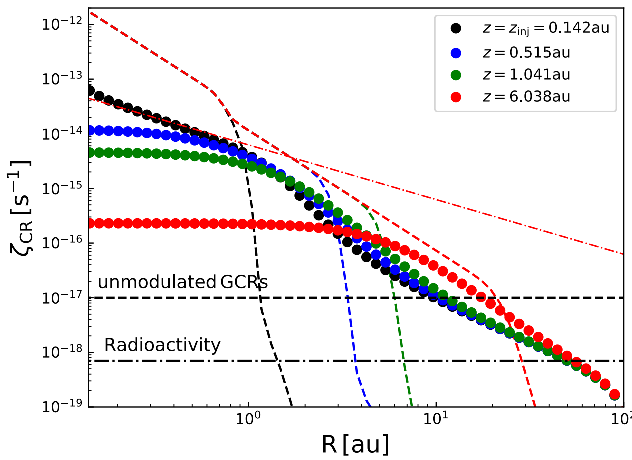

Figure 4. Radial ionization rate profile for a MMSN-type disc that has $p = 2.75$ and $\rho_0 \sim 1.4 \times 10^{-9}\,\mathrm{g\,cm^{-3}}$.

blue and green dots in Fig. 3) the corresponding radial ionization rate profiles are very similar to the profile obtained using the mean value of $p = 1.25$ (the black dots). Generally though for a fixed disc mass, steeper disc density profiles result in the stellar cosmic rays being attenuated more. For the most extreme case, corresponding to the MMSN value of $p = 2.75$, $\zeta_{CR} > 10^{-17}\mathrm{s^{-1}}$ only out to $R \sim 50$ au. The radial profile, as shown by the red dots in Fig. 3, deviates from the $1/r$ profile within R ∼1 au. Therefore, as will be discussed in more detail in Section 3.5, massive discs combined with steep density profiles will be very effective in impeding the transport of low-energy cosmic rays far out in the disc. The important point to note is that for the mean disc mass and the observed range of values of p considered, therefore not considering the (extreme) MMSN value of p, the cosmic rays are not significantly attenuated by the disc.

3.4 MMSN-type disc

The MMSN is a model that defines the minimum mass and distribution of material as a function of radius in a disc required to reproduce the distribution of planets in the Solar system in their current locations (Hayashi 1981). This model assumes that the planets in the Solar system formed at their current locations without migrating. The resulting parameters are that the radial extent of the protosolar disc was $R = 0.35$–36 au with $\rho_0 = 1.4 \times 10^{-9}\,\mathrm{g\,cm^{-3}}$ and $p = 2.75$ that gives $M_{disc} = 0.013\mathrm{M_\odot}$.

The simulation that we refer to as an ‘MMSN-type’ disc has $\rho_0 = 1.4 \times 10^{-9}\,\mathrm{g\,cm^{-3}}$ and $p = 2.75$ but retains the radial extent that we use for all of our simulations, $R = 0.1$–100 au. This means $M_{disc} = 0.024\mathrm{M_\odot}$ which is at the upper end of the observed disc mass distribution for solar mass stars. This steep density profile combined with the large disc mass means that the low-energy cosmic rays are unable to travel further than ∼10 au in the disc, shown in Fig. 4. A protoplanetary disc with these parameters would be an observational outlier. This MMSN-type disc has the same mass as the simulation shown by the green dots in Fig. 2. By comparing with the ionization rate given by the black dots in Fig. 4 it is clear that the value of p for discs this massive has a large effect. The dashed lines in Fig. 4 represent the X-ray ionization rate, as in Fig. 1, for the same vertical heights above the disc mid-plane as shown for the stellar cosmic rays. For this MMSN-type disc, the stellar X-rays dominate as the source of ionization out to 30 au. The low-energy cosmic rays

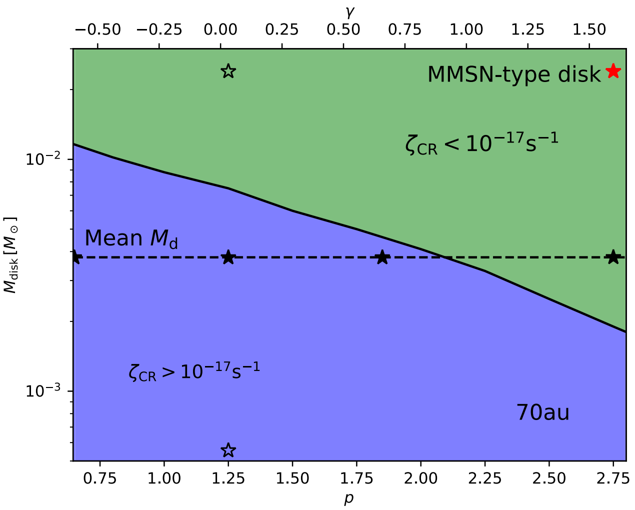

Figure 5. This plot shows two shaded regions as a function of M_{disc} and p. The blue shaded region represents simulations with values of M_{disc} and p for which the ionization rate from low-energy stellar cosmic rays dominates over that expected from unmodulated galactic cosmic rays ($\zeta_{CR} > 10^{-17}s^{-1}$) at $R = 70$ au at the mid-plane of the disc. The green shaded region corresponds to those simulations where $\zeta_{CR} < 10^{-17}s^{-1}$. The dashed line shows the mean disc mass value ($3.78 \times 10^{-3}M_\odot$). The black stars represent the simulations discussed in Sections 3.1–3.3 and the red star represents the MMSN-type disc investigated in Section 3.4.

dominate in the very outer regions of this disc but still result in a very low ionization rate.

3.5 Global trends: the ionization rate due to stellar cosmic rays

The previous sections have focused on a number of individual simulations to give some insight into the effect of varying the disc mass and the disc radial profile. We now examine the results obtained by considering the overall suite of simulations. This allows us to infer the influence of stellar cosmic rays on the global population of observed protoplanetary discs around solar-mass stars. We perform this analysis by examining the ionization rate due to stellar cosmic rays at $z = 0.142$ au ($\sim$ disc mid-plane) and identify whether $\zeta > \zeta_{GCR} = 10^{-17}$ s^{-1} for each simulation. We make this comparison at a number of different radii.

Over the whole range of disc parameters, we have explored, stellar cosmic rays dominate the mid-plane ionization ($\zeta_{CR} > 10^{-17}$ s^{-1}) within the first 10 au of the disc. This means that irrespective of the disc density profile or the disc mass (for the observationally motivated ranges we investigated) that low-energy cosmic rays provide an important source of ionization out to 10 au at the mid-plane of the disc.

However, for a large number of discs the region where stellar cosmic rays dominate extends much further. For example, we determine that $\sim$50 per cent of the discs have $\zeta_{CR} > 10^{-17}$ s^{-1} at the mid-plane of the disc at $\sim$70 au. Fig. 5 shows the results of this comparison for $R = 70$ au. The blue shaded region indicates the region of parameter space for which the ionization rate from stellar cosmic rays is greater than 10^{-17} s^{-1} and the green shaded region shows where it is less than it.

The horizontal black dashed line in Fig. 5 denotes the mean disc mass for the Chamaeleon star-forming region, as discussed in Section 2. The filled black stars represent the simulations discussed in Section 3.3 that vary p for the mean disc mass. The unfilled stars represent the simulations discussed in Section 3.2 that vary the disc mass for the mean value of $p = 1.25$. The red star denotes the MMSN-type disc simulation with $\rho_0 \sim 1.4 \times 10^{-9}$g cm^{-3} and $p = 2.75$ (as described in Section 3.4).

Fig. 5 shows that for disc masses between $M_{disc} \sim 2 \times 10^{-3}$ and $1 \times 10^{-2}M_\odot$ at a radius of 70 au the density profile of the disc is an important quantity. Variations in p result in the ionization rate due to stellar cosmic rays becoming bigger or smaller in comparison to the ionization rate due to unmodulated galactic cosmic rays at the disc mid-plane. Interestingly, the mean disc mass observed in Chamaeleon for a solar mass star, shown by the black dashed line in Fig. 5, lies within this region of parameter space. Thus, the level of ionization present in many discs will be very dependent on the density profile of the disc.

For more massive discs with $M_{disc} > 1 \times 10^{-2}M_\odot$, the ionization rate due to stellar cosmic rays is $<1 \times 10^{-17}$s^{-1} irrespective of the density profile of the disc at 70 au. Conversely, for less massive discs with $M_{disc} < 2 \times 10^{-3}M_\odot$ stellar cosmic rays dominate irrespective of the density profile of the disc for the values of p that we consider. For radii larger than 70 au, the number of simulations with $\zeta_{CR} > 10^{-17}$ s^{-1} decreases but remains significant, $\sim$25 per cent at 90 au for instance. The slope of the dividing line remains quite similar and shifts downwards.

4 DISCUSSION

We have performed a parameter space study of the disc mass and radial profile of the gas density to investigate the effect they have on the ionization from low-energy stellar cosmic rays. We have focused on the simplest case with mono-energetic low-energy cosmic rays assuming a value for the diffusion coefficient. Therefore, in this section we discuss the possible effect of including an energy spectrum of cosmic rays and the effect of varying the diffusion coefficient. We also compare with our previous results (Rodgers-Lee et al. 2017) and to other results in the literature.

4.1 Effect of varying the diffusion coefficient

In Section 3, we have assumed a diffusion coefficient of $D/c = 30r_L$ for 3 GeV protons. Fig. 6 in Rodgers-Lee et al. (2017) gives an overall picture of the effect of varying the diffusion coefficient for a very dense disc. As can be seen from this plot, increasing the diffusion coefficient results in a decrease in the ionization rate at small radii. At the same time, the radial profile of the ionization rate approaches a $1/r$ profile at larger radii for larger diffusion coefficients as the cosmic rays spend less time in the dense, and therefore more attenuating, inner region of the disc. In the absence of significant losses changing the diffusion coefficient would simply result in a vertical shift in the ionization profile with a $1/r$ profile throughout the system.

Relating to the results presented here the first point to note is that the effect of changing the diffusion coefficient will depend on the density profile of the disc. We can start with any of the simulations that resulted in a $1/r$ profile (such as Fig. 1 and many of the simulations in the blue shaded region of Fig. 5). We can estimate for these discs that the resulting change in the radial ionization rate obtained by increasing the diffusion coefficient will be a scaling law, since the steady state ionization rate for cases in which the diffusive escape time is shorter than the ionization loss time is $\zeta_{CR} \sim 1/Dr$. Larger diffusion coefficients than the value adopted for these cases are therefore expected to lead to a proportionally smaller steady-state ionization rate.

The effect of decreasing the diffusion coefficient may not be as simple. If the diffusion time becomes significantly longer than the ionization loss time-scale then behaviour similar to that seen in fig. 6 in Rodgers-Lee et al. (2017) may be observed. There the cosmic rays are absorbed faster than they can escape the dense inner regions of that disc that results in profiles steeper than $1/r$.

We can also consider the simulations occupying the green-shaded parameter space in Fig. 5 (such as the MMSN-type disc in Fig. 4) that already indicate, to some extent, radial ionization rate profiles steeper than $1/r$. It is possible for some of the discs in this parameter regime that increasing the diffusion coefficient will decrease the diffusion time sufficiently such that the low-energy cosmic rays will be able to reach the outer regions of the disc (such as the most massive disc simulation, shown as the green dots in Fig. 2, since it is not as far from a $1/r$ profile as Fig. 4, for instance). On the other hand, decreasing the diffusion coefficient for discs in this parameter regime will again result in even steeper radial profiles, as mentioned above.

4.2 Effect of including an energy spectrum of cosmic rays

We have only investigated mono-energetic stellar cosmic rays in this paper for simplicity. Again, the effect of including an energy spectrum of cosmic rays was investigated in Rodgers-Lee et al. (fig. 7, 2017). As evidenced by this plot the behaviour that results by including an energy spectrum of cosmic rays is complicated and will depend on the density profile of the disc. We will consider the energy spectrum used in Rodgers-Lee et al. (2017) that assumed a spectral index of -2 with stellar cosmic rays of energies from $\sim$100 MeV to 300 GeV. We can briefly comment that discs that exist in the green shaded region of Fig. 5 may become more ionized further out in the disc due to the high-energy component present in the energy spectrum.

4.3 Comparison to previous work

The main finding in Rodgers-Lee et al. (2017) was that low-energy cosmic rays were strongly attenuated by the dense protoplanetary disc. They were only competitive with unmodulated galactic cosmic rays as a source of ionization out to a maximum radius of $\sim$1 au. This is in contrast to the behaviour reported in this paper. The important difference is the assumed density profile and normalizing density. The disc investigated in Rodgers-Lee et al. (2017) had $\rho_0 = 2.33 \times 10^{-9}\,\mathrm{g\,cm^{-3}}$ and $p = 1.0$ which results in a very dense disc ($M_{\rm disc} \sim 0.1\mathrm{M}_\odot$ with a radial extent of 10 au as considered previously), outside of the parameter ranges that we investigated here. Such a dense and compact disc may exist but would be more representative of a more embedded, and therefore younger, source. On the other hand, some of the discs in Lupus observed in CN with ALMA shown in van Terwisga et al. (2019) are thought to have very small disc radii, $R \sim 15$ au but none of them are quite as massive as the disc we previously considered. Again, it is worth noting that massive optically thick compact discs may exist and remain undetected in ALMA surveys.

Thus, the parameters we vary here to investigate the ionizing influence of low-energy cosmic rays are likely to be more representative of the majority of protoplanetary discs. Our results indicate that for 50 per cent of the simulations that varied the disc masses and density profiles that low-energy stellar cosmic rays would be an important source of ionization out to 70 au in radius very close to the mid-plane. We also showed that an MMSN-type disc (with a larger disc mass than the MMSN disc model as a result of the outer radius being extended to 100 au while retaining the same values for p and ρ_0) would be an observational outlier, since the disc is quite massive in combination with a very steep density profile. The MMSN-type disc we investigated was very effective at preventing stellar cosmic rays from penetrating deep into the disc at large radii.

4.4 Comparison to the literature

Rab et al. (2017) present their stellar cosmic ray energy spectrum as a differential intensity in their figs 1 and 2. This has the advantage of being able to make a direct comparison with the local interstellar spectrum of galactic cosmic rays measured by Voyager (Stone et al. 2013) at 122 au and with the modulated galactic cosmic ray spectrum measured at 1 au on Earth (*PAMELA* measurements from 2006 to 2009; Adriani et al. 2013, for instance). Their assumed energy spectrum is based on observed solar energy particle spectra. They take one such spectrum from Mewaldt et al. (2005), divide by the flare duration, and multiply it by 10^5 to obtain their stellar energy particle spectrum. This results in a total energy injection rate of $10^{30}\,\mathrm{erg\,s^{-1}}$ with the majority of cosmic rays having MeV energies. In comparison, we inject a power ($L_{\rm CR} \sim 10^{28}\,\mathrm{erg\,s^{-1}}$) of only 3 GeV protons. There are a number of reasons that we find the low-energy cosmic rays to be more effective as a source of ionization in comparison to Rab et al. (2017).

First, the ionization loss rate for MeV protons is much larger than for GeV protons (see fig. 5.6 of Longair 2011). This means, despite the power used in Rab et al. (2017) being two orders of magnitude larger than used here, that the MeV protons are not able to travel as far as GeV protons in the disc, as they suffer larger energy losses. Secondly, their assumption of rectilinear propagation results in a steeper radial profile than the $1/r$ profile we recover for many of our simulations. Finally, the disc density profile and other physical parameters ($M_* = 0.7\mathrm{M}_\odot$ and $M_{\rm disk} = 0.01\,M_\odot$, for instance) are different and so it is difficult to make direct comparisons. None the less, the above reasons highlight that the overall power injection of cosmic rays is not necessarily an indication of what the ionization rate will be and that the energy of the cosmic rays is more important, combined with the assumption of their transport mechanism.

As mentioned in Section 1, Cleeves et al. (2015) constrain the total ionization rate for the disc of TW Hya ($\sim$0.8$\mathrm{M}_\odot$ CTTS) to be $\zeta \lesssim 10^{-19}\mathrm{s^{-1}}$. They find a total gas mass for the disc of $0.04 \pm 0.02\mathrm{M}_\odot$ with an assumed value of $\gamma = 1$. The density profile also assumes an exponential cut-off radius of 150 au which is $>$100 au ($R_{\rm out}$ for our discs) and therefore our density profiles should be similar within this radius. It is also important to note that our value of $\gamma = 1$ assumes a particular value of q, and therefore p, which is also different from that used in Cleeves et al. (2015). Changing q will result in the scale height of the disc changing.

By comparing with the observations presented in Pascucci et al. (2016) it is apparent that TW Hya's disc is relatively massive. The most massive disc that we consider ($2 \times 10^{-2}\mathrm{M}_\odot$) with $\gamma = 1$ has $\zeta_{\rm CR} \lesssim 10^{-19}\mathrm{s^{-1}}$ for $R > 80$ au for all heights above the disc. If the disc mass were doubled, then $\zeta_{\rm CR} \lesssim 10^{-19}\mathrm{s^{-1}}$ should occur at smaller radii. It is important to note that we consider a solar mass star, whereas TW Hya has a mass of $\sim$0.8$\mathrm{M}_\odot$. This will alter the above estimate by changing the scale height of the disc. None the less, the observational constraint on the ionization rate for TW Hya is not inconsistent with our results and as we have shown the ionization rate depends sensitively on the disc mass.

Fraschetti et al. (2018) perform test particle numerical simulations of the transport of $\sim$GeV stellar cosmic rays through the wind of a T Tauri star. They find that the ionizing effect of the cosmic rays occurs in only localized regions of the disc (specifically when they are the dominant source of ionization in comparison to X-rays) and close to the region of injection. Fraschetti et al. (2018) inject the cosmic rays at various radii between $2 - 10\,R_{*}(= 0.009 - 0.04\,\mathrm{au})$ which is within the truncation radius of the disc. In their case, the cosmic rays propagate until their trajectories intersect with the disc surface (and lose all their energy at the interaction point) or take them back to the stellar surface. This would be equivalent to assuming a very large density for the disc in our case which is why our earlier results in Rodgers-Lee et al. (2017) appeared consistent with their findings.

The work of Fraschetti et al. (2018) highlights that the ionization rate is possibly not symmetric around the axis of rotation of the star. By comparing with our results, it suggests that the cosmic rays need to be injected outside of the truncation radius in order to be able to significantly ionize the disc further out.

5 CONCLUSIONS

In this paper, we have assessed the ionizing effect of low-energy cosmic rays in protoplanetary discs originating close to the central star while varying the disc mass and the radial density profile of the disc. The variation in these parameters was motivated by current observations of protoplanetary discs (Pascucci et al. 2016; Tazzari et al. 2017).

We found that the $1/r$ profile expected for spherically symmetric diffusion, in the absence of significant energy losses, was recovered for many of the simulations in the parameter space that we investigated. This is in contrast to the results presented in Rodgers-Lee et al. (2017) because of the assumed normalizing density at 1 au. Effectively, we previously investigated a dense and compact disc which is likely to be an outlier for protoplanetary disc populations. Whereas, in this paper we have focused on values around the mean observed disc mass.

We found that the low-energy stellar cosmic rays provide an ionization rate greater than expected from unmodulated and unattenuated galactic cosmic rays out to a radius of ${\sim}10$ au near the mid-plane of the disc for all the simulations. For at least 50 per cent of the simulations, the low-energy cosmic rays continued to effectively ionize the mid-plane of the disc out to a radius of ${\sim}70$ au.

The mean disc mass, taken from dust observations of protoplanetary discs in the Chamaeleon star-forming region, combined with the mean value for the radial dust density profile index, lies within the parameter space of discs that display high levels of ionization, relative to that expected from unmodulated galactic cosmic rays, at 70 au. In comparison, the maximum disc mass (within the 1σ scatter expected from observations) results in the ionization rate decreasing by approximately an order of magnitude at 70 au.

The MMSN-type disc that we investigated (with a radial extent of 100 au instead of 36 au which results in $M_{\mathrm{disc}} \sim 0.024\mathrm{M}_{\odot}$) has a steep disc density profile and is quite massive in comparison to observed protoplanetary discs. This combination of parameters meant that this MMSN-type disc is one of the most effective discs at excluding low-energy cosmic rays from the outer regions of the disc.

Our results are consistent, within the uncertainties of our model parameters, with the observational constraint of an ionization rate of $\zeta \lesssim 10^{-19}\mathrm{s}^{-1}$ for TW Hya (Cleeves et al. 2013), since this represents a massive disc with a relatively steep radial density profile. Our results indicate that for less massive discs, which are more representative of the majority of discs around young solar-mass stars, the ionization rate due to low-energy cosmic rays should be much more significant.

Overall, we find that low-energy stellar cosmic rays may be an important source of ionization for many protoplanetary discs around young solar mass stars. An increase in the ionization rate at the mid-plane of the disc may have interesting consequences for the MRI and for the launching height of magnetocentrifugally launched winds.

ACKNOWLEDGEMENTS

This work has made use of the University of Hertfordshire's high-performance computing facility. DRL acknowledges funding from the Irish Research Council. We thank Antonella Natta for many interesting and helpful discussions. We thank the anonymous reviewer for their constructive comments.

REFERENCES

Adriani O. et al., 2013, ApJ, 765, 91
Ainsworth R. E., Scaife A. M. M., Ray T. P., Taylor A. M., Green D. A., Buckle J. V., 2014, ApJ, 792, L18
Ansdell M. et al., 2016, ApJ, 828, 46
Ansdell M. et al., 2018, ApJ, 859, 21
Bai X.-N., 2014, ApJ, 791, 137
Bai X.-N., Goodman J., 2009, ApJ, 701, 737
Balbus S. A., Hawley J. F., 1991, ApJ, 376, 214
Béthune W., Lesur G., Ferreira J., 2017, A&A, 600, A75
Blandford R. D., Payne D. G., 1982, MNRAS, 199, 883
Chiang E., Murray-Clay R., 2007, Nat. Phys., 3, 604
Cleeves L. I., Adams F. C., Bergin E. A., 2013, ApJ, 772, 5
Cleeves L. I., Bergin E. A., Qi C., Adams F. C., Öberg K. I., 2015, ApJ, 799, 204
Donati J.-F., Paletou F., Bouvier J., Ferreira J., 2005, Nature, 438, 466
Ercolano B., Glassgold A. E., 2013, MNRAS, 436, 3446
Fraschetti F., Drake J. J., Cohen O., Garraffo C., 2018, ApJ, 853, 112
Fromang S., Terquem C., Balbus S. A., 2002, MNRAS, 329, 18
Gaches B. A. L., Offner S. S. R., 2018, ApJ, 861, 87
Gammie C. F., 1996, ApJ, 457, 355
Glassgold A. E., Najita J., Igea J., 1997, ApJ, 480, 344
Gressel O., Turner N. J., Nelson R. P., McNally C. P., 2015, ApJ, 801, 84
Hayashi C., 1981, Prog. Theor. Phys. Suppl., 70, 35
Lesur G., Kunz M. W., Fromang S., 2014, A&A, 566, A56
Longair M. S., 2011, High Energy Astrophys., Cambridge Univ. Press, Cambridge
Mewaldt R. A. et al., 2005, J. Geophys. Res. (Space Phys.), 110, A09S18
Miotello A., et al., 2017, A&A, 599, A113
O'Keeffe W., Downes T. P., 2014, MNRAS, 441, 571
Padovani M., Hennebelle P., Marcowith A., Ferrière K., 2015, A&A, 582, L13
Padovani M., Marcowith A., Hennebelle P., Ferrière K., 2016, A&A, 590, A8
Padovani M., Ivlev A. V., Galli D., Caselli P., 2018, A&A, 614, A111
Pascucci I. et al., 2016, ApJ, 831, 125
Rab C., Güdel M., Padovani M., Kamp I., Thi W.-F., Woitke P., Aresu G., 2017, A&A, 603, A96
Rodgers-Lee D., Ray T. P., Downes T. P., 2016, MNRAS, 463, 134
Rodgers-Lee D., Taylor A. M., Ray T. P., Downes T. P., 2017, MNRAS, 472, 26
Schwarz K. R., Bergin E. A., Cleeves L. I., Zhang K., Öberg K. I., Blake G. A., Anderson D., 2018, ApJ, 856, 85
Stone E. C., Cummings A. C., McDonald F. B., Heikkila B. C., Lal N., Webber W. R., 2013, Science, 341, 150
Tazzari M. et al., 2017, A&A, 606, A88
Turner N. J., Drake J. F., 2009, ApJ, 703, 2152
Umebayashi T., Nakano T., 1981, PASJ, 33, 617
Umebayashi T., Nakano T., 2009, ApJ, 690, 69
van Terwisga S. E. et al., 2019, A&A, 623, A150
Wardle M., 2007, Ap&SS, 311, 35

APPENDIX: RESOLUTION STUDY

We perform a resolution study using the $||\ell||_2$ norm for the standard disc parameters with $\rho_0 = 6.8 \times 10^{-13}$ g cm^{-3} and $p = 1.25$, shown in Fig. A1. The radial and vertical extent of the disc remain the same, as given in Section 2.3.3. The cosmic rays are all injected at the same position and the $||\ell||_2$ norm is calculated at the same time for each of the simulations. The $||\ell||_2$ norm is defined as

$$||\ell(a, b)||_2 = \sqrt{\frac{1}{n}\sum_{i=0}^{n} |x_{i,a} - x_{i,b}|^2}, \tag{A1}$$

where the index i indicates the spatial position and the indices a, b correspond to two simulations with different resolutions. Five resolutions are considered increasing the number of bins in the radial (and vertical) directions with $N_\mathrm{r}(= N_\mathrm{z}) = 30, 40, 60, 90, 120$. A plot of $||\ell(a, b)||_2$ on a log–log scale should yield a straight line with a slope of -1 for our scheme since, although it is second order in space, it is first order in time and the solutions have not reached a steady state. The least-squared fitted slope of the data gives -0.95, indicating that the code is converging as expected. Furthermore, the fractional difference of the cosmic ray number density between any two resolutions is less than 10^{-3} everywhere. We therefore conclude that our results are well resolved.

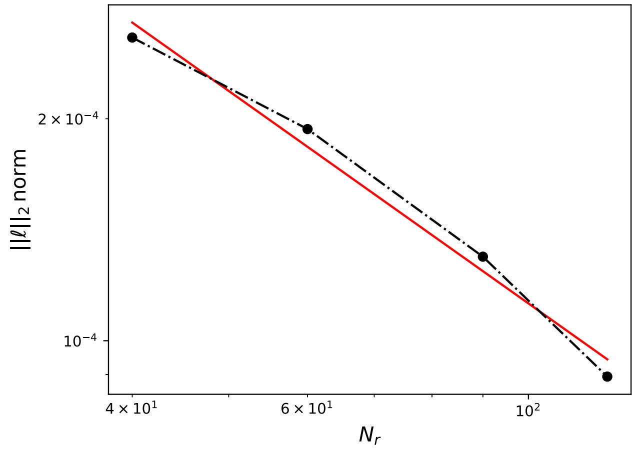

Figure A1. $||\ell||_2$ norm plotted as a function of resolution, where N_r is the number of grid zones in the radial direction. The number of cells in the vertical direction is also equal to N_r.

This paper has been typeset from a TEX/LATEX file prepared by the author.